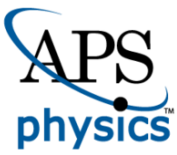

Novel Magnetic Block States in Low-Dimensional Iron-Based Superconductors

J. Herbrych, J. Heverhagen, N. D. Patel, G. Alvarez, M. Daghofer, A. Moreo, and E. Dagotto

Phys. Rev. Lett. **123**, 027203 — Published 10 July 2019

DOI: 10.1103/PhysRevLett.123.027203

Prediction of Magnetic Block States in Quasi-One-Dimensional Quantum Materials in the Orbital Selective Mott Phase

J. Herbrych[1,2,3], J. Heverhagen[4,5], N. D. Patel[6], G. Alvarez[7], M. Daghofer[4,5], A. Moreo[1,2], and E. Dagotto[1,2]
[1] *Department of Physics and Astronomy, University of Tennessee, Knoxville, Tennessee 37996, USA*
[2] *Materials Science and Technology Division, Oak Ridge National Laboratory, Oak Ridge, Tennessee 37831, USA*
[3] *Department of Theoretical Physics, Faculty of Fundamental Problems of Technology, Wrocław University of Science and Technology, 50-370 Wrocław, Poland*
[4] *Institute for Functional Matter and Quantum Technologies, University of Stuttgart, Pfaffenwaldring 57, D-70550 Stuttgart, Germany*
[5] *Center for Integrated Quantum Science and Technology, University of Stuttgart, Pfaffenwaldring 57, D-70550 Stuttgart, Germany*
[6] *Department of Physics, Ohio State University, Columbus, Ohio 43210, USA and*
[7] *Computational Sciences and Engineering Division and Center for Nanophase Materials Sciences, Oak Ridge National Laboratory, Oak Ridge, Tennessee 37831, USA*

Inelastic neutron scattering recently confirmed the theoretical prediction of a ↑↑↓↓-magnetic state along the legs of quasi-one-dimensional (quasi-1D) iron-based ladders in the orbital-selective Mott phase (OSMP). We show here that electron-doping of the OSMP induces a whole class of novel block-states with a variety of periodicities beyond the previously reported $\pi/2$ pattern. We discuss the magnetic phase diagram of the OSMP regime that could be tested by neutrons once appropriate quasi-1D quantum materials with the appropriate dopings are identified.

Introduction. Competing interactions in strongly correlated electronic systems can induce novel and exotic effects. For example, in the iron-based superconductors [1–4] charge, spin, and orbital degrees of freedom combine phenomena known from cuprates with those found in manganites. Prominent among these novel effects is the orbital-selective Mott phase (OSMP) [5], where interactions acting on a multi-orbital Fermi surface cause the selective localization of electrons on one of the orbitals. As a consequence, the system is in a mixed state with coexisting metallic and Mott-insulating bands [Fig. 1(a)]. Since the theoretical studies of the OSMP require the treatment of challenging multi-orbital models most of the investigations thus far were performed with approximations such as the the slave-particle mean field method [7–9, 43] or dynamical mean-field theory [10–12]. Here, we present unambiguous numerical evidence of the OSMP within low-dimensional multi-orbital Hubbard models, unveiling a variety of new phases.

The magnetic ordering associated with the OSMP could be significantly different from that observed in cuprates. The latter are described by single-band Hamiltonians and the parent compounds order in a staggered antiferromagnetic fashion. However, recent inelastic neutron scattering (INS) experiments [13] on quasi-1D iron-based materials of the 123 family (AFe_2X_3; A alkali metals, X=Se,S chalcogenides) unveiled exotic $\pi/2$-block magnetic states where spins form antiferromagnetically (AFM) coupled ferromagnetic (FM) islands, in a ↑↑↓↓-pattern [Fig. 1(b)]. Similar patterns were also reported in two dimensions with iron vacancies, such as in $Rb_{0.89}Fe_{1.58}Se_2$ [14] and $K_{0.8}Fe_{1.6}Se_2$ [8, 15–17]. For the aforementioned compounds the OSMP state is believed to be relevant [8, 13, 18–20].

Recent theoretical investigations [21, 22] showed that a multi-orbital Hubbard model in the OSMP state properly describes the INS spin spectra of $\pi/2$-block state of powder $BaFe_2Se_3$ [13]. However, the origin of block magnetism and its relation to the OSMP is an intriguing and generic question that has been barely explored. We show that the block-OSMP magnetism can develop in various shapes and sizes depending on the electron-doping, far beyond the previously reported $\pi/2$-pattern. Moreover, here we develop effective Hamiltonians for the OSMP which allows for an intuitive understanding of the origin of block magnetism. Our simplified, yet accurate, model allows for reliable numerical investigations of the OSMP and predicts the behavior of the maximum of the spin structure factor in electron-doped OMSP.

Model. Our conclusions are based on extensive simulations of two- and three-orbital models in chain and ladder geometries for a variety of model parameters. For clarity, consider first the two-orbital 1D Hubbard model,

$$\begin{aligned} H_{\rm H} = &- \sum_{\gamma,\gamma',\ell,\sigma} t_{\gamma\gamma'} \left(c^{\dagger}_{\gamma,\ell,\sigma} c_{\gamma',\ell+1,\sigma} + {\rm H.c.} \right) + \Delta \sum_{\ell} n_{1,\ell} \\ &+ U \sum_{\gamma,\ell} n_{\gamma,\ell,\uparrow} n_{\gamma,\ell,\downarrow} + (U - 5J_{\rm H}/2) \sum_{\ell} n_{0,\ell} n_{1,\ell} \\ &- 2J_{\rm H} \sum_{\ell} \mathbf{S}_{0,\ell} \cdot \mathbf{S}_{1,\ell} + J_{\rm H} \sum_{\ell} \left(P^{\dagger}_{0,\ell} P_{1,\ell} + {\rm H.c.} \right) , \quad (1) \end{aligned}$$

where $c^{\dagger}_{\gamma,\ell,\sigma}$ creates an electron with spin $\sigma = \{\uparrow,\downarrow\}$ at orbital $\gamma = \{0,1\}$ and site $\ell = \{1,\ldots,L\}$. $t_{\gamma\gamma'}$ denotes a diagonal hopping amplitude matrix in orbital space γ, with $t_{00} = -0.5$ and $t_{11} = -0.15$ in eV units. The crystal-field splitting is $\Delta = 0.8$ eV (kinetic-energy band-

width is $W = 2.1$ eV). The local (γ, ℓ) orbital-resolved particle density is $n_{\gamma,\ell} = \sum_\sigma n_{\gamma,\ell,\sigma}$, $\mathbf{S}_{\gamma,\ell}$ is the local spin, and $P_{\gamma,\ell} = c_{\gamma,\ell,\uparrow} c_{\gamma,\ell,\downarrow}$ is the pair-hopping operator. The global filling is $n = N/L$, where N is the number of electrons and L the system size. U is the repulsive Hubbard interaction, while $J_{\rm H}$ is the Hund exchange, fixed here to $J_{\rm H} = U/4$ [21–28]. All results are obtained with the density matrix renormalization group method [29–33] with truncation errors smaller than $\sim 10^{-7}$. Open boundary conditions were assumed.

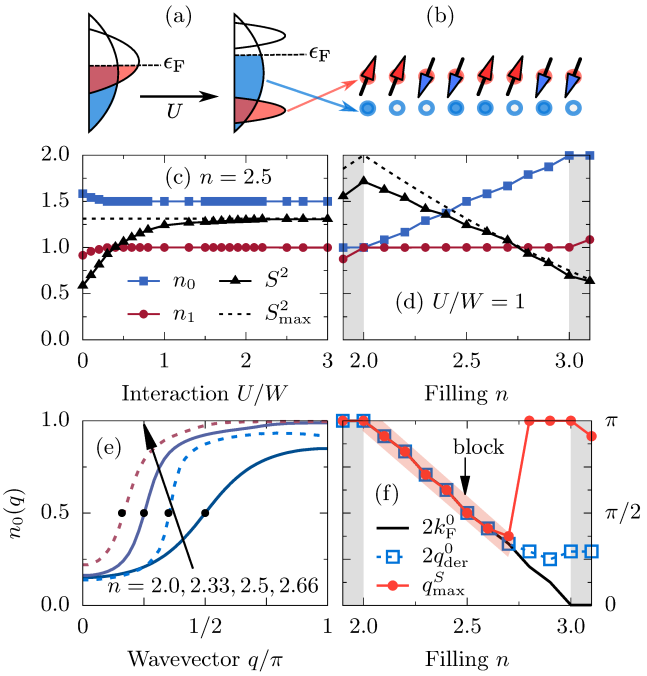

Figure 1. (Color online) Schematic representation of (a) the orbital-selective Mott phase and (b) $\pi/2$-block spin state. (c) Interaction U and (d) filling n dependence of the total magnetic moment $\langle S^2_\ell \rangle$ and orbital-resolved occupation numbers n_γ of the two-orbital Hubbard model Eq. (1), using $L = 48$ sites. In (d), the black dashed line represents the largest possible magnetic moment $S^2_{\rm max}$. (e) Momentum distribution function $n_0(q)$ of the $\gamma = 0$ orbital. Points indicate $q^0_{\rm der}$, the position of the maximum in $\mathrm{d}n_0(q)/\mathrm{d}q$. (f) n dependence of the position of the maximum of the spin structure factor $q^S_{\rm max}$. Block-OSMP is denoted as a colored area. In the same panel we also present the position of the orbital $\gamma = 0$ Fermi-vector calculated via $2k^0_{\rm F} = \pi n_0$ and via $2q^0_{\rm der}$.

Although the Hamiltonian Eq. (1) appears complex, it represents a generic SU(2) symmetric multiorbital system. As long as we are in the block-OSMP state, our results are *not* sensitive to details of the parameter sets: for example, in the Supplementary Material [34] we show that the same conclusions are drawn from a system with or without interorbital hybridization and with two or three orbitals. Ladder geometries also lead to similar findings. We also observe block states in the effective Kondo-Heisenberg model. Our results are thus generic and intrinsic of multi-orbital systems in the block-OSMP.

Orbital-selective Mott phase. Figures 1(c-d) present the orbital-resolved occupation numbers n_γ and the total magnetic moment per site squared $\langle S^2_\ell \rangle = S_\ell(S_\ell + 1)$. As expected in the OSMP, increasing the interaction U "locks" the occupation number of one of the orbitals to $n_1 = 1$. This behavior is observed in the $2 < n < 3$ region, yielding a remaining orbital $\gamma = 0$ only fractionally occupied. Simultaneously, $\langle S^2_\ell \rangle$ is almost fully saturated to its maximal value (given by the total filling) when $n_1 = 1$. Charge fluctuations $\delta n^2_\gamma = \langle n^2_\gamma \rangle - \langle n_\gamma \rangle^2$ [27, 34] indicate that the number of doublons is highly suppressed on the single-occupied orbital, different from the fractionally occupied orbital $\gamma = 0$ where $\delta n^2_0 \neq 0$ suggests metallic character. The results above, and the orbital-resolved density-of-states (DOS) analysis [34], are consistent with OSMP physics in a wide range $2 < n < 3$. As in previous investigations [27], our block-OSMP system is in an overall metallic state for all considered fillings, albeit with a highly reduced Fermi-level DOS. It is currently unknown if the latter approximates a pseudogap or rather a weak insulator, and more detailed analysis is needed.

Block magnetism. Previous efforts [21, 22] showed that the OSMP can display exotic magnetic properties, such as AFM coupled FM islands (the spin-block phase). Here, one of our main results is that the magnetic pattern of the block-OSMP is *not* limited to the $\pi/2$-phase, but remarkably the OSMP can support a variety of spin patterns previously unknown. Figure 2(a) illustrates the filling n dependence of the total spin structure factor $S(q)$ [35]. Several conclusions can be obtained from the displayed results at $U = W$: (i) below half-filling, $n < 2$, the (weak) maximum of $S(q)$ at $q = \pi$ indicates a paramagnetic state with short-range spin staggered tendencies. (ii) Entering the OSMP phase, $2 < n < 3$, robust correlations develop with well-defined peaks in $S(q)$ at $q^S_{\rm max}$ [see Fig. 3(a,b) and [34] for finite-size scaling]. In this region $q^S_{\rm max}$ strongly depends on n, and decreases as n increases [see also Fig. 1(f)]. (iii) For $n > 3$ paramagnetism is recovered with a (weak) maximum at $q = \pi$ [36]. Although the strong spin correlations unveiled here resemble long-range order, it is expected that in 1D eventually they would decay slowly as a power law. However, weak couplings perpendicular to the chains/ladders should stabilize the unveiled orders into long-range patterns with the same local block order as reported here.

Consider now the real-space correlation functions $\langle \mathbf{S}_\ell \cdot \mathbf{S}_{L/2} \rangle$ [Fig. 2(a), top]. Starting with $n = 2$, the structure factor has a "standard" π-AFM staggered spin pattern, common of Mott insulators. However, at $n \simeq 2.3$ an unexpected novel spin pattern emerges involving 1- and 2-sites FM islands of the form $\uparrow\uparrow\downarrow\uparrow\downarrow\downarrow\uparrow\downarrow$. At $n = 2.5$ the previously known AFM coupled FM blocks of two spins, $\uparrow\uparrow\downarrow\downarrow$, is stabilized. Increasing further the electron doping, the magnetic islands continue growing in size. On the considered $L = 48$ lattice, the largest new pattern ob-

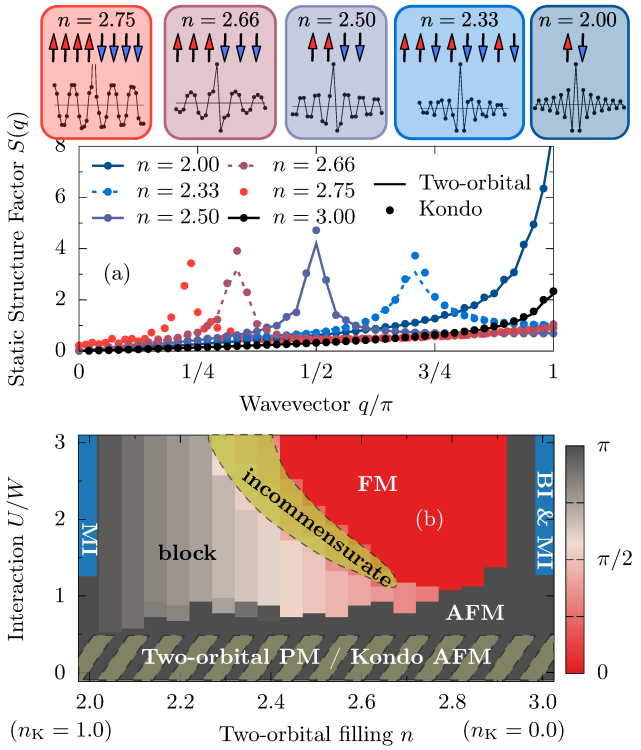

Figure 2. (Color online) (a) Static structure factor $S(q)$ for various fillings n at fixed $U = W$, for the two-orbital Hubbard (lines) and generalized Kondo-Heisenberg (points) models, both using $L = 48$ sites ($L = 72$ for $n = 2.75$, see text for details). Real-space correlation functions $\langle \mathbf{S}_\ell \cdot \mathbf{S}_{L/2} \rangle$ of the two-orbital Hubbard model and sketches of the spin alignment are also presented at the top. (b) Interaction vs filling magnetic phase diagram of the generalized Kondo-Heisenberg model on $L = 48$ sites. The dashed-shaded area represents the region where the mapping is not valid.

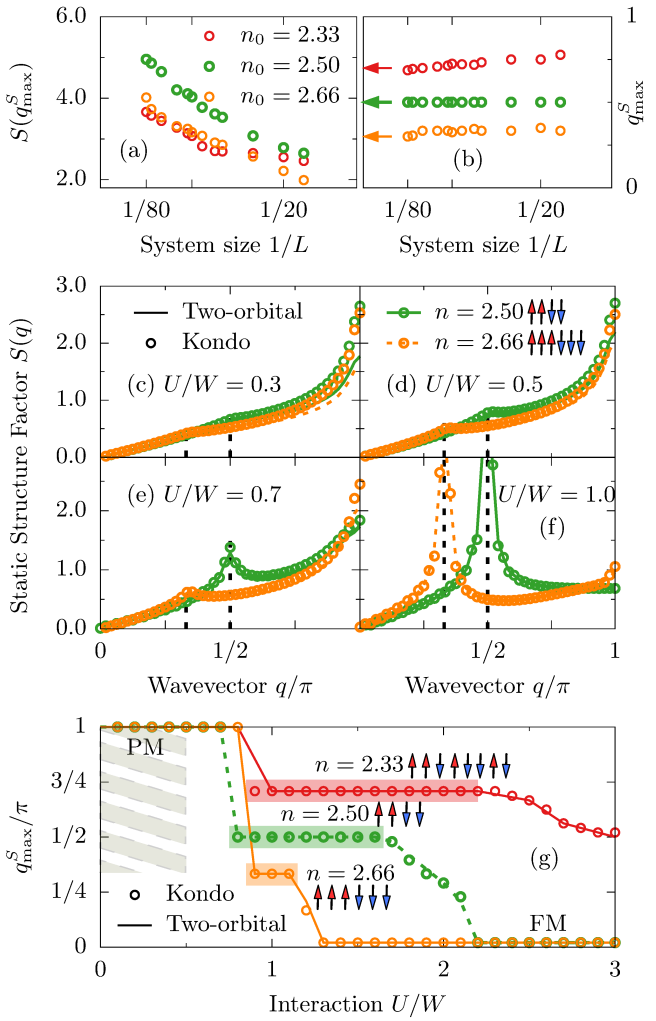

Figure 3. (Color online) (a,b) Finite-size scaling of (a) the spin structure factor maximum $S(q^S_{\rm max})$ and (b) position of $q^S_{\rm max}$, calculated for $U/W = 1$ using the generalized Kondo-Heisenberg model. Arrows in (b) represent the $L \to \infty$ limit πn_0. (c-f) U dependence of $S(q)$ for $n = 2.50$ and 2.66. Lines (circles) represent results using the two-orbital Hubbard model (generalized Kondo-Heisenberg model) and $L = 48$ sites. Dashed horizontal lines represent $2k_{\rm F} = \pi n$. (g) U dependence of $q^S_{\rm max}$ for the two-orbital Hubbard model (lines) and generalized Kondo-Heisenberg model (circles) at fillings $n = 2.33\,, 2.50$, and 2.66. The dashed-shaded area represents the region where the mapping is not valid.

served contains FM blocks with three spins ($\uparrow\uparrow\uparrow\downarrow\downarrow\downarrow$) for $n \simeq 2.66$. Increasing n further, $S(q)$ suddenly reaches a maximum again at $q^S_{\rm max} = \pi$. As shown later, for large enough L, larger FM islands were observed [37], albeit in narrower regions of the parameter space.

Effective model. To better understand these surprisingly rich new magnetic structures, let us consider an effective Hamiltonian. Because in the OSMP the double occupancy of the localized orbital $\gamma = 1$ with $n_1 = 1$ is highly suppressed, it is natural to restrict - using the Schrieffer-Wolff transformation [38] - the Hilbert space of Eq. (1) to the subspace with strictly one electron per site at $\gamma = 1$ orbital. The formal derivation is in [34], and here we just present the final result, i.e., the generalized Kondo-Heisenberg model defined as,

$$H_{\rm K} = t_{00} \sum_{\ell,\sigma} \left(c^\dagger_{0,\ell,\sigma} c_{0,\ell+1,\sigma} + {\rm H.c.} \right) + U \sum_\ell n_{0,\ell,\uparrow} n_{0,\ell,\downarrow} + K \sum_\ell \mathbf{S}_{1,\ell} \cdot \mathbf{S}_{1,\ell+1} - 2J_{\rm H} \sum_\ell \mathbf{S}_{0,\ell} \cdot \mathbf{S}_{1,\ell}\,, \qquad (2)$$

with $K = 4t^2_{11}/U$. The electronic filling of the effective Hamiltonian is either $n_{\rm K} = n - 1$ or $n_{\rm K} = 3 - n$ due to the particle-hole symmetry of Eq. (2). We tested the accuracy of Eq. (2) by comparing results for $S(q)$ in a wide range of parameters. From Figs. 2(a), 3, and 4(a), clearly the magnetic properties of the multi-orbital Hamiltonian in the block-OSMP are accurately reproduced by the generalized Kondo-Heisenberg model [39]. Furthermore, due to the small Hilbert space of the latter, we can accurately study much larger systems and stabi-

lize larger blocks. In Fig. 2(a) we show results for $L = 72$, $U/W = 1.02$, $J_{\rm H}/U = 0.27$, and $n_{\rm K} = 0.25$ which exhibit the block of 4-spins [40].

For $U = 0$ (and $K = 0$) the effective Hamiltonian resembles the widely-studied Kondo-Heisenberg (Kondo) model. In this framework, we can understand intuitively the origin of the magnetic blocks [41–43]. At half-filling $n_{\rm K} = 1$ and for a strong Kondo (Hund) coupling, $J_{\rm H} \gg K, t_{00}$, the $\gamma = 0$ electrons form local Kondo interorbital triplets with localized spins. Increasing the electrons' mobility, t_{00}, leads to the double-exchange FM ordering [44]. On the other hand, when $t_{00} \gg J_{\rm H}, K$ one can observe (short-range) features in the spin spectrum upon doping at twice the Fermi vector ($2k_{\rm F}$) of the itinerant orbitals, Fig. 3(c-d). In the OSMP, when $J_{\rm H} \sim K \sim \mathcal{O}(t_{00})$, the $2k_{\rm F}$ instability of itinerant orbitals is amplified leading to spin (quasi-)long-range order with maximum at $S(2k_{\rm F})$ [Fig. 3(e-f)]. As a consequence, competition of double- and super-exchange mechanisms leads to the formation of block magnetic islands. We tested the above "$2k_{\rm F}$ prediction" of the maximum of the spin structure factor by comparing $q^S_{\rm max}$ with the $U \to 0$ limit in 1D, i.e., $2k^0_{\rm F} = \pi n_0$. Also, we calculated the Fermi vector position directly from the momentum distribution function $n_\gamma(q)$ via the maximum $q^0_{\rm der}$ of $\mathrm{d}n_0(q)/\mathrm{d}q$ [Fig. 1(e) and [34]]. It is evident from Fig. 1(c) that the block-magnetism follows the Fermi vector of the $\gamma = 0$ orbital [45]. It is important to remark that the above "$2k_{\rm F}$-stabilization" is an *emergent phenomena* unique of multi-orbital systems. Doping the single-band Hubbard model leads only to short-ranged ordered spin correlations, retaining their π-AFM character. This is strikingly different from the behavior reported here in multi-orbital models because the Hund coupling between subsystems induces novel magnetic block-states.

As discussed above, the effective Hamiltonian Eq. (2) accurately describes the OSMP magnetic phases, and is in good agreement with the rich island-physics of Kondo-lattice Hamiltonians unveiled before [41, 48–51]. This allows us to create a detailed magnetic phase diagram of the effective model. In Fig. 2(b) we present the n–U dependence of $q^S_{\rm max}$ using $L = 48$ sites: (i) at $U < W/2$, where the mapping should not work, the system is paramagnetic; (ii) at $n < 2.5$ for all considered U's and for $U \simeq W$ at $n \lesssim 2.7$ we found the novel stable blocks of various sizes, depending on $k_{\rm F} \propto n$; (iii) finally at $U \gg W$ the system is ferromagnetic for all $2 < n < 3$ [see also Fig. 3(g)]. Furthermore, in between the FM and block phases we observed a narrow incommensurate magnetic region which will be studied in the future.

Ladder geometry. To confirm the robustness of our findings and to bring our results closer to experimental compounds, such as AFe_2X_3 [13, 18, 19, 46, 47, 52–54], consider now two-orbital ladder systems. The kinetic part of the Hamiltonian is defined with isotropic hoppings $t^{\parallel}_{\gamma\gamma'} = t^{\perp}_{\gamma\gamma'} = t_{\gamma\gamma'}$ and $\Delta = 1.6\,$eV (kinetic energy bandwidth $W_{\rm L} = 3.55\,$eV), while the remaining interactions are as in Eq. (1). Figure 4(a) presents the bonding $q_\perp = 0$ component of the spin structure factor $S(q_\parallel, 0)$ for $U = W_{\rm L}$. Consistent with the 1D predictions, the maximum of $S(q_\parallel, 0)$ strongly depends on filling. At $n = 2.5$ the system is in a π-AFM state, and with increasing filling spin blocks start to develop. Interestingly, our results indicate that as $n \to 2.5$ the legs are FM aligned. However, as $n \to 3$ a novel AFM ordering between the legs develop, while the FM islands involve three spins [55]. The latter may arise from competing double-exchange-FM vs AFM tendencies coming from the localized spins and Fermi instability $k_{\rm F}$, namely the energy of the large FM blocks as $n \to 3$ is reduced by the rung AFM arrangement. Thus, we speculate that the ladder geometry can stabilize even larger magnetic blocks due to the AFM ordering between legs.

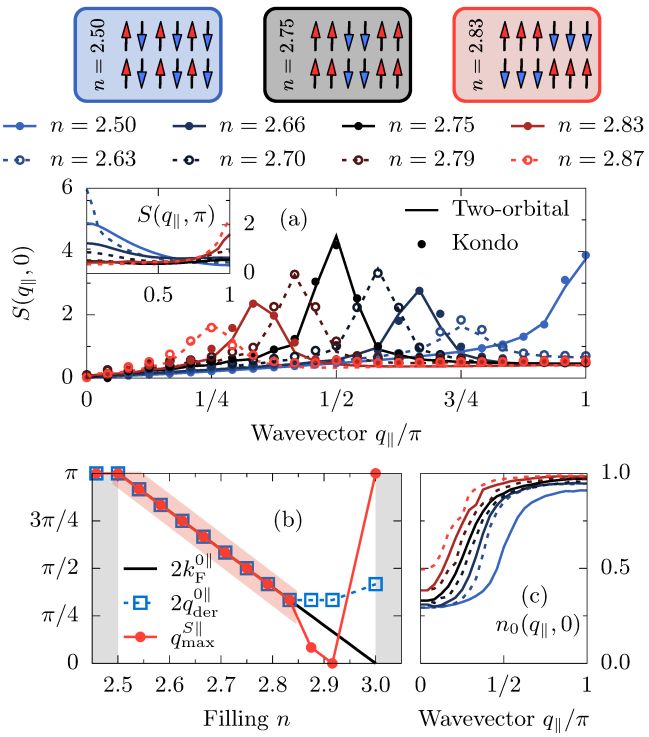

Figure 4. (Color online) (a) n dependence of $S(q_\parallel, 0)$ (bonding component) at $U = W_{\rm L}$ using the two-orbital Hubbard ladder (lines) and the generalized Kondo-Heisenberg (points) models, both on $L = 48$ sites (24 rungs). The inset depicts the antibonding component $S(q_\parallel, \pi)$. Schematics of the spin configurations are also presented. (b) Filling n dependence of $q^{S\parallel}_{\rm max}$, $2k^{0\parallel}_{\rm F} = 2\pi n_0$, and $2q^{0\parallel}_{\rm der}$. Block-OSMP appears as a colored area. (c) Momentum distribution function $n_0(q_\parallel, 0)$ of the $\gamma = 0$ orbital in the bonding $q_\perp = 0$ sector. The legend is the same as in (a).

Consider now the filling dependence of the maximum of the ladder spin structure factor $q^{S\parallel}_{\rm max}$. As in 1D, $q^{S\parallel}_{\rm max}$ follows the Fermi vector $q^{0\parallel}_{\rm der}$ estimated from the momentum distribution function [Fig. 4(b)]. Although the re-

gion where the block magnetism is observed, $2.5 < n < 3$, is smaller compared with chains, this can be explained considering the ladder $U \to 0$ limit prediction of Fermi vectors. In this case, for an isotropic ladder ($t^{\parallel}_{00} = t^{\perp}_{00}$) and $n > 1.5 + 1$, the itinerant orbital Fermi vector is $2k^{0\parallel}_{\rm F} = 2\pi n_0$ (as opposed to $2k^{0}_{\rm F} = \pi n_0$ for a chain). Figures 4(b,c) indicate excellent agreement between $2k^{0\parallel}_{\rm F}$ and the numerically evaluated $2q^{0\parallel}_{\rm der}$ [$\mathrm{d}n(q_\parallel, 0)/\mathrm{d}q$ maximum] in the OSMP. Furthermore, as in chains, the block-magnetism follows the $2k^{0\parallel}_{\rm F}$ prediction.

Conclusions. We have shown that the multi-orbital Hubbard model in the OSMP regime supports spin-block magnetism of various novel sizes and shapes, depending on filling and lattice geometry. Moreover, we also derived an effective OSMP Hamiltonian, the generalized Kondo-Heisenberg model, which describes all magnetic phases accurately. The observed spin structures are related to the $2k_{\rm F}$ of the metallic electron bands, but spin blocks are much more sharply defined than they would be in the mere sinusoidal structure arising from a weak-coupling Fermi-surface instability [see real-space spin correlations in Fig. 2(a) top] . We believe that the strongly correlated nature of the localized spins, due to its narrow bandwidth [25], enhances the $2k_{\rm F}$ instability in a manner only possible in OSMP regimes. Our predictions could be relevant within the 123 families of iron-based materials and can be confirmed by INS experiments. But we remark that our results are generic and could apply to any quasi-1D quantum material in an OSMP regime.

We thank C. Batista and N. Kaushal for fruitful discussions. J. Herbych, N. D. Patel, A. Moreo, and E. Dagotto were supported by the US Department of Energy (DOE), Office of Science, Basic Energy Sciences (BES), Materials Sciences and Engineering Division. J. Herbrych acknowledges also partial support by the Polish National Agency of Academic Exchange (NAWA) under contract PPN/PPO/2018/1/00035. G. Alvarez was partially supported by the Center for Nanophase Materials Sciences, which is a DOE Office of Science User Facility, and by the Scientific Discovery through Advanced Computing (SciDAC) program funded by U.S. DOE, Office of Science, Advanced Scientific Computing Research and Basic Energy Sciences, Division of Materials Sciences and Engineering. J. Heverhagen and M. Daghofer were supported by the Deutsche Forschungsgemeinschaft, via the Emmy-Noether program (DA 1235/1-1) and FOR1807 (DA 1235/5-1) and by the state of Baden-Württemberg through bwHPC.

[1] G. R. Stewart, Rev. Mod. Phys. **83**, 1589 (2011).
[2] E. Dagotto, Rev. Mod. Phys. **85**, 849 (2013).
[3] P. Dai, Rev. Mod. Phys. **87**, 855 (2015).
[4] R. M. Fernandes and A. V. Chubukov, Reports on Progress in Physics **80**, 014503 (2017).
[5] A. Georges, L. d. Medici, and J. Mravlje, Annu. Rev. Condens. Matter Phys. **4**, 137 (2013), and references therein.
[6] S. Biermann, L. de Medici, and A. Georges, Phys. Rev. Lett. **95**, 206401 (2005).
[7] Luca de Medici, S. R. Hassan, M. Capone, and X. Dai, Phys. Rev. Lett. **102**, 126401 (2009).
[8] R. Yu and Q. Si, Phys. Rev. Lett. **110**, 146402 (2013).
[9] R. Yu and Q. Si, Phys. Rev. B **96**, 125110 (2017).
[10] A, Koga, N. Kawakami, T. M. Rice, and M. Sigrist, Phys. Rev. Lett. **92**, 216402 (2004).
[11] E. Jakobi, N. Blümer, and P. van Dongen, Phys. Rev. B **87**, 205135 (2013).
[12] A. van Roekeghem, P. Richard, H. Ding, S. Biermann, C. R. Phys. **17**, 140 (2016).
[13] M. Mourigal, S. Wu, M. B. Stone, J. R. Neilson, J. M. Caron, T. M. McQueen, and C. L. Broholm, Phys. Rev. Lett. **115**, 047401 (2015).
[14] M. Wang, C. Fang, D.-X. Yao, G. Tan, L. W. Harriger, Y. Song, T. Netherton, C. Zhang, M. Wang, M. B. Stone, W. Tian, J. Hu, and P. Dai, Nat. Comm. **2**, 580 (2011).
[15] B. Wei, H. Qing-Zhen, C. Gen-Fu, M. A. Green, W. Du-Ming, H. Jun-Bao, and Q. Yi-Ming, Chin. Phys. Lett. **28**, 086104 (2011).
[16] Y.-Z. You, H. Yao, and D.-H. Lee, Phys. Rev. B **84**, 020406(R) (2011).
[17] R. Yu, P. Goswami, and Q. Si, Phys. Rev. B **84**, 094451 (2011).
[18] J. M. Caron, J. R. Neilson, D. C. Miller, K. Arpino, A. Llobet, and T. M. McQueen, Phys. Rev. B **85**, 180405(R) (2012).
[19] S. Dong, J.-M. Liu, and E. Dagotto, Phys. Rev. Lett. **113**, 187204 (2014).
[20] J.M. Pizarro and E.Bascones, Phys. Rev. Materials **3**, 014801 (2019).
[21] J. Rincón, A. Moreo, G. Alvarez, and E. Dagotto, Phys. Rev. Lett. **112**, 106405 (2014).
[22] J. Herbrych, N. Kaushal, A. Nocera, G. Alvarez, A. Moreo, and E. Dagotto, Nat. Comm. **9**, 3736 (2018).
[23] Z. P. Yin , K. Haule, and G. Kotliar, Nat. Mat. **10**, 932 (2010).
[24] P Dai, J. Hu, and E. Dagotto, Nat. Phys. **8**, 709 (2012).
[25] S. Li, N. Kaushal, Y. Wang, Y. Tang, G. Alvarez, A. Nocera, T. A. Maier, E. Dagotto, and S. Johnston, Phys. Rev. B. **94**, 235126 (2016).
[26] N. Kaushal, J. Herbrych, A. Nocera, G. Alvarez, A. Moreo, F. A. Reboredo, and E. Dagotto, Phys. Rev. B. **96**, 155111 (2017).
[27] N. D. Patel, A. Nocera, G. Alvarez, A. Moreo, S. Johnston, and E. Dagotto, arXiv:1807.10419 (2018).
[28] J. Rincón, A. Moreo, G. Alvarez, and E. Dagotto, Phys. Rev. B **90**, 241105(R) (2014).
[29] S. R. White, Phys. Rev. Lett. **69**, 2863 (1992).
[30] S. R. White, Phys. Rev. B **48**, 10345 (1993).
[31] U. Schollwöck, Rev. Mod. Phys. **77**, 259 (2005).
[32] G. Alvarez, Comput. Phys. Commun. **180**, 1572 (2009).
[33] More technical details about these calculations can be found at g1257.github.io/papers/88.
[34] See Supplementary Material for: (i) analysis of the OSMP, (ii) additional results for the spin structure factor $S(q)$ for systems with interorbital hybridization and for the three-orbital model, (iii) details of the mapping to the generalized Kondo-Heisenberg model, and (iv) ad-

ditional results for the momentum distribution function $n_\gamma(q)$.

[35] We use standard standard open boundary conditions definitions of the wavevectors $q = \pi k/(L+1)$ with $k = 1, \ldots, L$ and $S(q) = [2/\pi/(L+1)] \sum_{\ell,m} \exp[iq(\ell - m)] \langle \mathbf{S}_\ell \cdot \mathbf{S}_m \rangle$.

[36] Note that in this doping region the orbital $\gamma = 0$ is in a band-insulator state, while the electrons on the $\gamma = 1$ orbital are itinerant ($\delta n_1^2 > 0$).

[37] On the other hand, patterns with $q^S_{\rm max} \to \pi/L$ ($n \to 3 - 1/L$) are not possible since this would lead (in the extreme) to nonphysical cases involving just one domain wall in the system (spin block of $L/2$ spins).

[38] J. R. Schrieffer and P. A. Wolff, Phys. Rev. **149**, 491 (1966).

[39] The effective Hamiltonian properly describes also other OSMP magnetic phases, such as ferromagnetism at $U \gg W$ [34]. However, we remark that Eq. (2) is valid *only* in the OSMP regime. For $U \to 0$ both orbitals of the multi-orbital system have metallic character, the magnetic moments are not fully developed (Fig. 1), and the system is paramagnetic (PM).

[40] In this case we have included small Ising-like anisotropy in the localized spins, i.e., $0.83K^\perp = K^z$, which helps to stabilize the block pattern.

[41] C. D. Batista, J. M. Eroles, M. Avignon, and B. Alascio, Phys. Rev. B **58**, R14 689 (1998).

[42] D. J. Garcia, K. Hallberg, C. D. Batista, M. Avignon, and B. Alascio, Phys. Rev. Lett. **85**, 3720 (2000).

[43] S. Biermann, L. de Medici, and A. Georges, Phys. Rev. Lett. **95**, 206401 (2005).

[44] E. Dagotto, T. Hotta, and A. Moreo, Physics Reports **344**, 1 (2001), and references therein.

[45] It is also interesting to note that $k^0_{\rm F} \neq q^0_{\rm der}$ for the same filling $n \gtrsim 2.7$ for which we observe the breakdown of the magnetic blocks.

[46] J. M. Caron, J. R. Neilson, D. C. Miller, A. Llobet, and T. M. McQueen, Phys. Rev. B **84**, 180409(R) (2011).

[47] Y. Nambu, K. Ohgushi, S. Suzuki, F. Du, M. Avdeev, Y. Uwatoko, K. Munakata, H. Fukazawa, S. Chi, Y. Ueda, and T. J. Sato, Phys. Rev. B **85**, 064413 (2012).

[48] H. Aliaga, B. Normand, K. Hallberg, M. Avignon, and B. Alascio, Phys. Rev. B **64**, 024422 (2001).

[49] J. C. Xavier, E. Novais, and E. Miranda, Phys. Rev. B **65**, 214406 (2002).

[50] D. J. Garcia, K. Hallberg, C. D. Batista, S. Capponi, D. Poilblanc, M. Avignon, and B. Alascio, Phys. Rev. B **65**, 134444 (2002).

[51] D. J. Garcia, K. Hallberg, B. Alascio, and M. Avignon, Phys. Rev. Lett. **93**, 177204 (2004).

[52] T. Hawai, Y. Nambu, K. Ohgushi, F. Du, Y. Hirata, M. Avdeev, Y. Uwatoko, Y. Sekine, H. Fukazawa, J. Ma, S. Chi, Y. Ueda, H. Yoshizawa, and T. J. Sato, Phys. Rev. B **91**, 184416 (2015).

[53] S. Chi, Y. Uwatoko, H. Cao, Y. Hirata, K. Hashizume, T. Aoyama, and K. Ohgushi, Phys. Rev. Lett. **117**, 047003 (2016).

[54] M. Wang, S. J. Jin, Ming Yi, Yu Song, H. C. Jiang, W. L. Zhang, H. L. Sun, H. Q. Luo, A. D. Christianson, E. Bourret-Courchesne, D. H. Lee, Dao-Xin Yao, and R. J. Birgeneau, Phys. Rev. B **95**, 060502(R) (2017).

[55] See also D.R. Neuber, M. Daghofer, A.M. Oleś, and W. von der Linden, physica status solidi (c), **3**, 32 (2006).